Turkish Journal of Chemistry

Volume 49 | Number 4 Article 9

8-18-2025

Influence of synthesis parameters on the structural formation of mayenite via the citrate sol-gel method

BÜŞRA ERYILDIRIM

NURAY OKTAR

DORUK DOĞU

Follow this and additional works at: https://journals.tubitak.gov.tr/chem

 Part of the Chemistry Commons

Recommended Citation

ERYILDIRIM, B, OKTAR, N, & DOĞU, D (2025). Influence of synthesis parameters on the structural formation of mayenite via the citrate sol-gel method. *Turkish Journal of Chemistry 49* (4): 479-494. https://doi.org/10.55730/1300-0527.3746



This work is licensed under a Creative Commons Attribution 4.0 International License.
This Research Article is brought to you for free and open access by TÜBİTAK Academic Journals. It has been accepted for inclusion in Turkish Journal of Chemistry by an authorized editor of TÜBİTAK Academic Journals. For more information, please contact academic.publications@tubitak.gov.tr.

TÜBİTAK

Turkish Journal of Chemistry

http://journals.tubitak.gov.tr/chem/

Research Article

Turk J Chem
(2025) 49: 479-494
© TÜBİTAK
doi:10.55730/1300-0527.3746

Influence of synthesis parameters on the structural formation of mayenite via the citrate sol-gel method

Büşra ERYILDIRIM[1], Nuray OKTAR[2], Doruk DOĞU[3,*]

[1]Department of Chemical Engineering, Graduate School of Natural and Applied Sciences, Gazi University, Ankara, Turkiye
[2]Department of Chemical Engineering, Faculty of Engineering, Gazi University, Ankara, Turkiye
[3]Department of Metallurgical and Materials Engineering, School of Engineering, Atılım University, Ankara, Turkiye

Received: 18.02.2025 • **Accepted/Published Online:** 02.07.2025 • **Final Version:** 19.08.2025

Abstract: Mayenite ($Ca_{12}Al_{14}O_{33}$) has remarkable properties such as high oxygen mobility, ionic conductivity, and catalytic activity. It has many different applications, including oxide-conducting electrolytes, fluorescent lamps, moisture sensors, hydrogen-permeable membranes, oxygen pumps, hydrogen storage, and catalysis. However, pure and homogeneous mayenite synthesis parameters have not yet been fully explored. This study examines the effect of synthesis parameters including metal salt (MS) to citric acid (CA) molar ratios (1:1 and 1:2), pH (0.4–2), and calcination temperature (900–1200 °C) in citrate sol-gel method on the crystal structure of mayenite. Synthesized materials were examined by thermogravimetric (TG), X-ray diffraction (XRD), X-ray photoelectron spectroscopy (XPS), Raman spectroscopy, N_2 adsorption-desorption, scanning electron microscopy (SEM), inductively coupled plasma-optical emission spectrometry (ICP-OES), Fourier-transform infrared spectroscopy (FTIR), and pyridine adsorbed diffuse reflectance Fourier-transformed infrared spectroscopy (DRIFTS) analyses. The results show that all 3 parameters contribute to the mayenite phase formation and different impurity phases can be observed depending on the synthesis parameters. With no pH adjustment and an MS to CA ratio of 1, other phases of calcium aluminate mostly form. Mayenite becomes the main phase by doubling the CA amount. Besides CA, pH is also an important factor in mayenite synthesis. When the pH was adjusted to 2 with the MS to CA ratio at 1:1, mayenite was formed as the main phase, but other phases of calcium aluminate were also observed in the structure. XRD results show that all parameters studied influence the crystal structure of the final material, including the calcination temperature. This study shows that pure mayenite can be synthesized with a calcination temperature of 1200 °C, at a pH of 2, and the MS to CA molar ratio of 1:2.

Key words: Mayenite, sol-gel, calcination temperature, pH, metal salt to citric acid ratio

1. Introduction

Mayenite ($Ca_{12}Al_{14}O_{33}$) is a remarkable material that is used in many technological applications such as oxide-conducting electrolytes, fluorescent lamps, moisture sensors, hydrogen-permeable membranes, oxygen pumps, hydrogen storage, H_2 production from photocatalytic water splitting, and catalytic reactions. This is due to the high oxygen mobility, ionic conductivity, and catalytic properties of mayenite [1–6]. Mayenite is an electrical insulator with a band gap of approximately 7 eV. It can be transformed into an electroactive functional material at low temperatures, such as a metallic conductor with a low work function but high superconductivity and chemical inertness [3]. These extraordinary properties can be attributed to its crystal structure. The crystal structure of mayenite is similar to that of zeolites and clathrate phases of ice, but the positively charged (4+) framework of the unit cell of mayenite is not the same. Mayenite has a crystal structure that can be defined as a nanoporous cubic structure with a unit cell edge of 11.98 Å and 2 Z (formula units) [7–9]. In simple terms, the structure is a framework of AlO_4 tetrahedra attached to the corner by connections bridged by Ca. The Ca-Al-O framework forms a total of 12 interconnected cages. This framework comprises 32 of the 33 oxygen anions; the extra one is distributed randomly in 1/6 of the large cages within the framework [10]. These oxygen ions, known as extra framework oxygen ions, are loosely bound to the lattice. Six cage-wall Ca^{2+} ions encircle each free oxygen atom with an interionic spacing 1.5× greater than that of the free oxygen in the CaO case. This spacing confirms that oxygen ions are loosely bonded in cages since it is twice the O^{2-} ionic radii (0.24 nm) [3]. These extra framework oxygen ions lead to high oxygen mobility and ionic conductivity. By replacing them with other anions such as OH^-, N^{3-}, Au, Cl^-, and F^-, various physical and chemical properties can be achieved, increasing the applications of mayenite [5,10–14].

* Correspondence: doruk.dogu@atilim.edu.tr

This work is licensed under a Creative Commons Attribution 4.0 International License.

Mayenite is a mineral that can be found in nature. To obtain pure mayenite in large quantities, it can be synthesized artificially by different methods. The solid-state synthesis route is a simple and conventional method for mayenite synthesis; however, it requires long reaction times and high temperatures (above 1200 °C) [14–21]. Sol-gel synthesis is a promising alternative method for mayenite synthesis because homogeneous and pure mayenite can be obtained at lower temperatures than the solid-state route, and the morphology of the synthesized materials can be controlled and modified easily [22]. Materials with well-defined and homogeneous crystal morphologies can be obtained by sol-gel synthesis [23–25]. In addition, sol-gel synthesis enables doping of the material structure with different ions or metals [2,26].

In the literature, the sol-gel method has been used in the synthesis of nano/meso particles, ceramic-added geopolymers, and nanocomposites. The effects of synthesis parameters on the structure have also been investigated [27–30]. The addition of ceramic additives to geopolymer and nanocomposite systems leads to significant improvements in the thermal, mechanical, and chemical properties of the materials [31]. The unique properties of mayenite, such as high temperature resistance and high electrical conductivity can be used to improve the properties of geopolymers and nanocomposites. Composites containing mayenite and graphene oxide have multifunctional properties, including optical, electrochemical, dielectric, and mechanical properties suitable for high-performance multifunctional applications such as smart cement materials [32].

Although mayenite has many uses, indepth examination of the synthesis parameters is limited. Most of the literature reports on the different uses of mayenite and the impurities found in the structure. Moreover, all synthesis parameters are not clearly defined in these publications. The sol-gel method for mayenite synthesis generally consists of the following steps: hydrolysis of the precursor, condensation, gelling, aging, drying, and calcination. Each of these steps is very important to produce the desired final material. In the sol-gel method, the final structure of the synthesized material is significantly affected by the nature and concentration of precursors, the type of solvent and acidity of the medium, the concentration of each species in the solvent, aging time and temperature, and calcination time and temperature. During the synthesis of mayenite by the sol-gel method, these parameters are very important for the formation of the desired structure because calcium oxide (CaO), aluminum oxide (Al_2O_3), and other mixed oxide phases containing aluminum and calcium ($Ca_3Al_2O_6$, $CaAl_2O_4$, $CaAl_4O_7$, $Ca_5Al_6O_{14}$, etc.) can also form depending on the synthesis parameters. The ratio of starting materials for mayenite synthesis is fixed at a Ca to Al molar ratio of 12:14. Due to their low cost, nitrate forms of metals were chosen as starting materials, and deionized water was used as a solvent. Citric acid, tartaric acid, glycolic acid, and oxalic acid are popular chelating agents used in the sol-gel process of material synthesis. Citric acid was selected as the chelating agent for this investigation because it is readily available, affordable, and an effective and extensively utilized chelating agent in the sol-gel process [33]. In material synthesis studies using the citrate sol-gel process, the molar ratio of metal salt (MS) to citric acid (CA) is an important parameter affecting the gel formation rate and homogeneity [34]. In addition, some studies have reported that changing the pH of the solution with ammonia or ethylenediamine increases the binding of the cation to citrate. In this regard, the stability and homogeneity of metal citrate solutions largely depend on solution pH [33,35]. Therefore, it was decided to adjust the pH with ethylenediamine and study the effect of the MS to CA molar ratio to optimize the formation of stable and homogeneous metal citrate species. In the $CaO\text{-}Al_2O_3$ phase diagram, mayenite forms at 900 °C and above, and other phases of calcium aluminate can also be found in the structure at these temperatures [36]. To obtain pure mayenite, the effect of calcination temperature on the final structure was also investigated. In summary, the effect of MS to CA molar ratio, pH, and calcination temperature were examined in this study to synthesize the pure mayenite structure. The crystal structures of the materials synthesized with different parameters were determined by X-ray diffraction (XRD) analysis. Thermogravimetric (TG), Fourier-transform infrared spectroscopy (FTIR), pyridine adsorbed diffuse reflectance Fourier-transformed infrared spectroscopy (DRIFTS), N_2 adsorption-desorption analysis, scanning electron microscopy (SEM) analysis, laser Raman spectroscopy, X-ray photoelectron spectroscopy (XPS), and inductively coupled plasma-optical emission spectrometry (ICP-OES) analysis were also performed. This study clearly presents the mayenite synthesis parameters and provides the optimum synthesis route by determining the effect of the parameters on the final structure. In most mayenite synthesis studies, the synthesis parameters are not specified, and the resulting material may contain impurities. In addition, there are no studies examining the effects of the MS to CA molar ratio, pH, and calcination temperature together with detailed analysis techniques. In this respect, the findings of this study will be a valuable resource for other researchers who need to synthesize pure mayenite.

2. Materials and methods

2.1. Preparation of materials

Mayenite materials were synthesized by a citrate sol-gel procedure [35] using the following steps: preparation of the MS solution, gel formation, drying, and calcination. In this procedure, the starting materials calcium nitrate tetrahydrate

($Ca(NO_3)_2.4H_2O$, Merck, Darmstadt, Germany) and aluminum nitrate tetrahydrate ($Al(NO_3)_3.9H_2O$, Merck, Darmstadt, Germany) were dissolved in deionized water (50 mL) at room temperature to obtain a Ca to Al molar ratio of 12:14. The total concentration of the resulting solution was 1 M. The solution was then heated to 60 °C under continuous stirring. The CA solution used as a chelating agent was prepared in another beaker. Enough CA ($C_6H_8O_7$, Sigma-Aldrich, St. Louis, MO, USA) was added to deionized water (50 mL) to obtain a total MS to CA molar ratio of 1:1 or 1:2. The CA solution was added to the MS solution under continuous stirring at 60 °C in a dropwise manor. At this stage, the desired pH (1 or 2) of the solution was adjusted with ethylenediamine ($C_2H_4(NH_2)_2$, Sigma-Aldrich, St. Louis, MO, USA). Synthesis without pH adjustment was also tested in this study. After pH adjustment, the temperature was increased to 85–90 °C and kept at this temperature under continuous stirring until a viscous gel was formed (after about 2h). The obtained gel was then dried in the oven at 130 °C for 12 h to obtain a cake-like structure. This cake-like structure was pulverized to obtain a powder. Finally, the powder was calcined under a flow of dry air. All samples were heated to the calcination temperature with a ramp rate of 5 °C/min from room temperature and calcined in a tube furnace at the desired calcination temperature (900, 1000, 1100, and 1200 °C) for 4 h. A schematic representation of the synthesis of mayenite by the citrate sol-gel method is given in Figure 1.

2.2. Characterization of the synthesized materials

TG analyses of the synthesized materials were carried out at the Central Laboratory of Ankara Yıldırım Beyazıt University. Analyses were performed on a HITACHI STA 7300 instrument (Tokyo, Japan). TG analyses were carried out at temperatures between 25 and 1200 °C with a heating rate of 5 °C/min under dry air flow.

To analyze the crystal structure of the synthesized materials, XRD analysis was conducted using a Bruker D2 Phaser diffractometer (Billerica, MA, USA) with a Cu, K_α (λ = 0.15406 nm) radiation source at the Metal Forming Center of Excellence (MFCE) in Atılım University. XRD analyses were performed between the 2θ range of 10°–90° with a scanning speed of 2°/min. Crystal sizes of the synthesized materials were calculated using the Scherrer equation ($L = K\lambda/\beta\cos\theta$). In this equation, L, the crystal size, is a measure of the dimension of the particle in the direction perpendicular to the reflecting plane; K is the shape factor depending on the sphericity of the crystal that is commonly taken as 0.89 as in this study; λ is the X-ray wavelength (0.15406 nm); β is the full width at half maxima in radian of the strongest peak (2θ approximately 18° is taken); and θ is the Bragg angle, the angle between the incident beam and the reflecting plane that leads to constructive interference of X-ray beams and hence a peak is observed [37].

FTIR and pyridine adsorbed DRIFTS analyses were performed using a JASCO Model FT/IR-4700 instrument (Tokyo, Japan). Laser Raman spectroscopy analyses were performed at room temperature using a JASCO NRS4500 Raman spectrometer (Tokyo, Japan) with a 532 nm ion laser.

XPS analysis using a PHI 5000 VersaProbe (ULVAC-PHI, Kanagawa, Japan) instrument was performed to define the surface chemistry of the materials. Data was collected for C 1s, O 1s, Al 2p, and Ca 2p regions, and peak correction was made for the C 1s peak at 284.5 eV. XPSPEAK41 software was used for curve fitting.

N_2 adsorption-desorption analysis was performed using a Micromeritics Tristar II 3020 device (Norcross, GA, USA) at 77 K within P/P_o values from 10^{-5} to 0.99 to obtain the surface areas of synthesized materials. Synthesized materials were degassed under a vacuum at 250 °C for 2 h before analysis.

SEM analysis was performed with the HITACHI SU5000 field emission high-resolution scanning electron microscope (Tokyo, Japan) to assign the morphology of the synthesized materials. Metal ratios of the synthesized materials were assigned by ICP-OES analysis with a PerkinElmer Optima 4300DV instrument (Waltham, MA, USA).

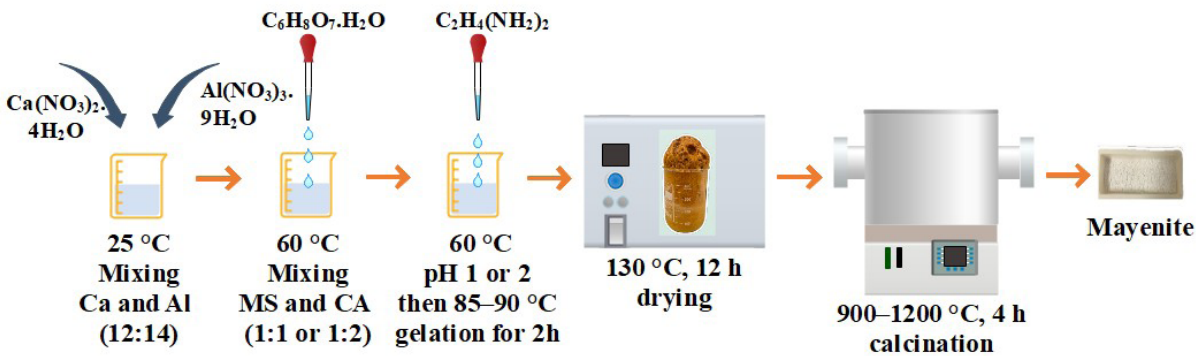

Figure 1. A schematic diagram of the citrate sol-gel method for mayenite synthesis.

3. Results and discussion

3.1. Results of synthesized materials with a MS to CA ratio of 1

The synthesis studies were first carried out by keeping the MS to CA molar ratio at 1 with no pH adjustment (pH of 0.6). After that, the effect of pH was also tested by adjusting the pH to 2 by adding ethylenediamine to the solution.

TG analyses were conducted between 25–1200 °C with a heating rate of 5 °C/min under dry airflow and nitrogen flow (Figure 2). TG analysis showed weight losses of up to 200 °C due to water removal from the material structure. Weight losses between 250–950 °C occurred due to nitrate decomposition and the combustion of other organic compounds [2,12,38]. The mass of the material became stable in a dry air atmosphere at approximately 950 °C. Below 950 °C, all metal nitrate compounds are completely decomposed, and above this temperature, solid-solid reactions occur between calcium oxide and alumina. According to the CaO-Al_2O_3 phase diagram, the possible phases above 1000 °C are $Ca_{12}Al_{14}O_{33}$, $Ca_3Al_2O_6$, $CaAl_2O_4$, and $CaAl_4O_7$ [36]. In the XRD analysis results, these phases were present in the structure (Figure 3). Mass loss continued in the nitrogen atmosphere after 950 °C. In addition, the final powder after TG analysis under nitrogen flow was observed to be black in color, indicating carbon compounds remain in the structure. Therefore, synthesis studies were continued in a dry air atmosphere.

XRD patterns (2θ range of 10°–90°) of materials synthesized without pH adjustment at different calcination temperatures from 900 to 1200 °C for 4 h are shown in Figure 3. Characteristic peaks of mayenite were not observed in the XRD patterns of the synthesized materials at 900 and 950 °C. $Ca_3Al_2O_6$ (COD 9014359) [39] and $CaAl_2O_4$ (COD 2002888) [40] phases, which are the usual impurities formed during mayenite synthesis, were mainly formed. XRD pattern of mayenite presents the characteristic peaks of mayenite around 2θ values of 18.1°, 30°, 33.4°, 36.7°, 41.2°, 46.7°, 55.2°, and 57.4° (COD 2102955) [41,42]. At 1000 °C, a characteristic peak of mayenite (2θ approximately 18°) was observed with low peak intensity. This low peak intensity indicates that mayenite is not the main structure in this synthesized material.

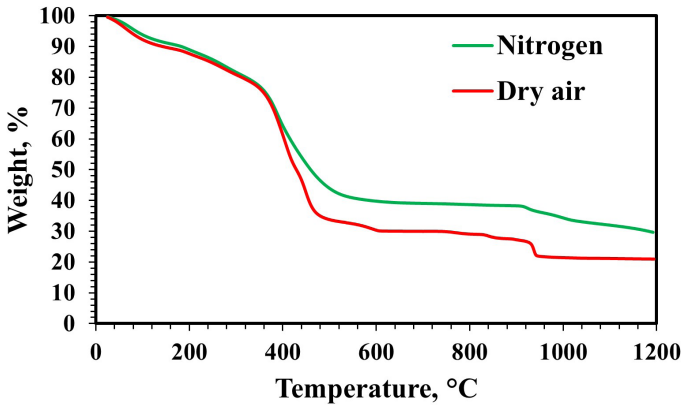

Figure 2. TG analysis results of the material synthesized without pH adjustment (MS:CA 1:1, pH of 0.6).

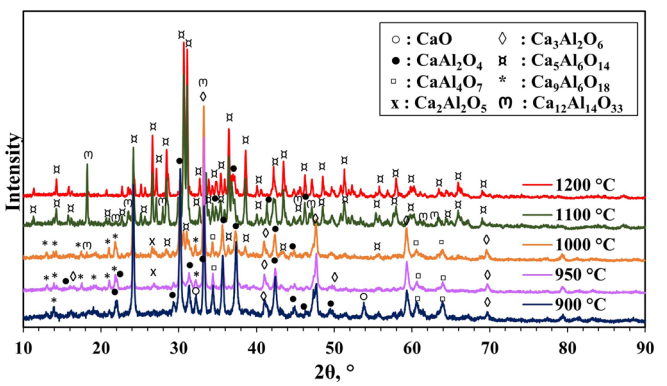

Figure 3. XRD patterns of materials synthesized without pH adjustment and calcined at different temperatures (900–1200 °C) for 4 h (MS:CA 1:1, pH of 0.6).

At 1100 °C, mainly $Ca_5Al_6O_{14}$ (COD 2106611) [43] was observed, and the peak intensities of this phase and the mayenite phase increased. At 1200 °C, the $Ca_5Al_6O_{14}$ phase was formed and the mayenite phase disappeared at this temperature.

The phases and percent crystallinity of the synthesized material obtained at different calcination temperatures are given in Table 1. Phases and crystallinities of the synthesized materials were determined with the DIFFRAC.EVA program, the Bruker D2 Phaser diffractometer software. By comparing the signal to noise ratio in these diffractograms, one can observe that the crystallinity increases with increasing calcination temperature, as expected.

To examine the effect of pH, it was adjusted to 2 while the MS to CA ratio was kept at 1. Contrary to the material without pH adjustment, the mayenite phase was formed at all temperatures after calcination was carried out between 900 and 1200 °C. Impurities ($Ca_5Al_6O_{14}$, $Ca_3Al_2O_6$, and $CaAl_2O_4$) formed in addition to the mayenite main phase according to the XRD patterns (Figure 4 and Table 1). Intiso et al. [44] also detected $Ca_3Al_2O_6$ and $CaAl_2O_4$ phases in the mayenite. They

Table 1. Phases identified and crystallinity using X-ray powder diffraction.

MS/CA	1				1/2					
Calcination Temperature, °C	Phases Present		Crystallinity, %		Phases Present			Crystallinity, %		
	pH: 0.6	pH: 2	pH:0.6	pH:2	pH: 0.43	pH: 1	pH: 2	pH: 0.43	pH: 1	pH: 2
900	CaO, $CaAl_2O_4$, $CaAl_4O_7$, $Ca_3Al_2O_6$, $Ca_9Al_6O_{18}$	$CaAl_2O_4$, $Ca_3Al_2O_6$, $Ca_{12}Al_{14}O_{33}$	73	76	$CaAl_2O_4$, $Ca_{12}Al_{14}O_{33}$	$CaAl_2O_4$, $Ca_5Al_6O_{14}$, $Ca_{12}Al_{14}O_{33}$	$CaAl_2O_4$, $Ca_{12}Al_{14}O_{33}$	78	74	83
950	$CaAl_2O_4$, $CaAl_4O_7$, $Ca_2Al_2O_5$, $Ca_3Al_2O_6$, $Ca_9Al_6O_{18}$	-	76	-	-	-	$CaAl_2O_4$, $Ca_{12}Al_{14}O_{33}$	-	-	85
1000	$CaAl_2O_4$, $CaAl_4O_7$, $Ca_2Al_2O_5$, $Ca_3Al_2O_6$, $Ca_5Al_6O_{14}$, $Ca_9Al_6O_{18}$, $Ca_{12}Al_{14}O_{33}$	$CaAl_2O_4$, $Ca_3Al_2O_6$, $Ca_{12}Al_{14}O_{33}$	78	79	$CaAl_2O_4$, $Ca_{12}Al_{14}O_{33}$	$CaAl_2O_4$, $Ca_{12}Al_{14}O_{33}$	$CaAl_2O_4$, $Ca_{12}Al_{14}O_{33}$	84	82	84
1100	$CaAl_2O_4$, $Ca_5Al_6O_{14}$, $Ca_9Al_6O_{18}$, $Ca_{12}Al_{14}O_{33}$	$Ca_5Al_6O_{14}$, $Ca_{12}Al_{14}O_{33}$	80	80	$CaAl_2O_4$, $Ca_{12}Al_{14}O_{33}$	$CaAl_2O_4$, $Ca_{12}Al_{14}O_{33}$	$CaAl_2O_4$, $Ca_5Al_6O_{14}$, $Ca_{12}Al_{14}O_{33}$	84	85	82
1200	$Ca_5Al_6O_{14}$	$CaAl_2O_4$, $Ca_5Al_6O_{14}$, $Ca_{12}Al_{14}O_{33}$	81	79	$CaAl_2O_4$, $Ca_{12}Al_{14}O_{33}$	$CaAl_2O_4$, $Ca_{12}Al_{14}O_{33}$	$Ca_{12}Al_{14}O_{33}$	86	87	87

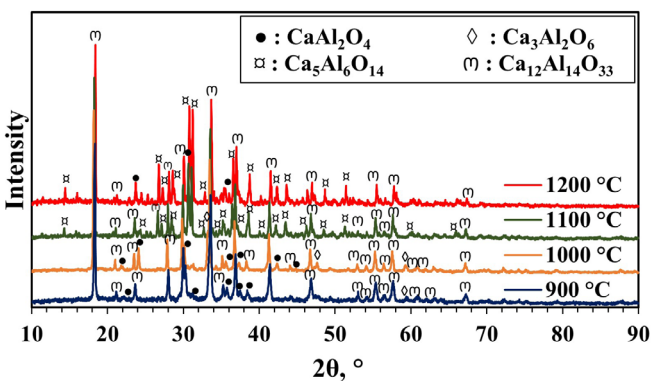

Figure 4. XRD patterns of materials synthesized with pH adjustment and calcined at different temperatures (900–1200 °C) for 4 h (MS:CA 1:1, pH of 2).

used the citrate sol-gel method for synthesis. The crystal sizes of the synthesized mayenite phases at different calcination temperatures were calculated using the Scherrer equation. The crystal size of the material was 79.6 nm and was not affected by changing the calcination temperature at the pH value of 2. Crystallinity increased slightly with increasing calcination temperature.

3.2. Results of synthesized materials with a MS to CA ratio of 1:2

The next set of experiments focused on synthesis studies done at a MS to CA molar ratio of 1:2. Synthesis studies were carried out without pH adjustment (pH: 0.43) and by adjusting the pH level to 1 and 2 using ethylenediamine.

The XRD patterns of the materials synthesized with a pH of 0.43 are given in Figure 5. At 900 °C, there was a $CaAl_2O_4$ impurity phase in the material structure in addition to the mayenite phase. As the calcination temperature increased, the formation of $CaAl_2O_4$ phase decreased. Additionally, crystallinity increased with increasing the calcination temperature (Table 1). When the molar amount of CA was doubled (Figure 5), the mayenite phase was formed as the main phase at all temperatures compared to the material without pH adjustment (Figure 3). This result shows how important the amount of CA in the synthesis solution is for the final structure.

The XRD patterns of the materials synthesized with a pH of 1 are given in Figure 6. Similar to the results obtained in the material with a pH of 0.43, there was $CaAl_2O_4$ phase in addition to the mayenite phase in the material structure at 900 °C, and an almost pure mayenite phase was obtained with calcinations done above 1000 °C (Table 1). Additionally, a small amount of $Ca_5Al_6O_{14}$ phase was observed at 900 °C. Changing the calcination temperature did not cause a change in the crystal size (79.6 nm) of the material and the crystallinity of the material increased with increasing calcination temperature (Table 1).

The XRD patterns of the materials synthesized with a pH of 2 are given in Figure 7. The mayenite phase formed at 900, 950, 1000, and 1200 °C, along with a trace amount of the $CaAl_2O_4$ phase, which is a possible impurity during synthesis.

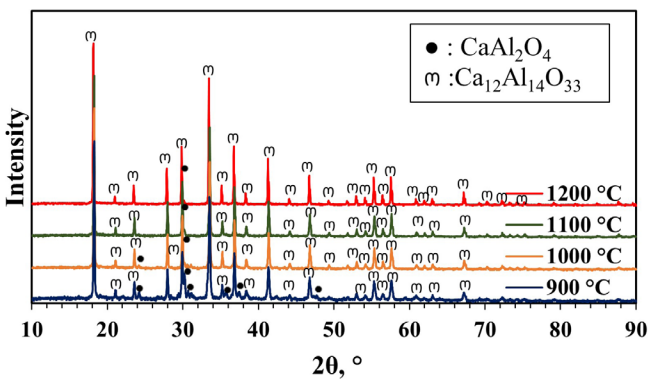

Figure 5. XRD patterns of materials synthesized without pH adjustment and calcined at different temperatures (900–1200 °C) for 4 h (MS:CA 1:2, pH of 0.43).

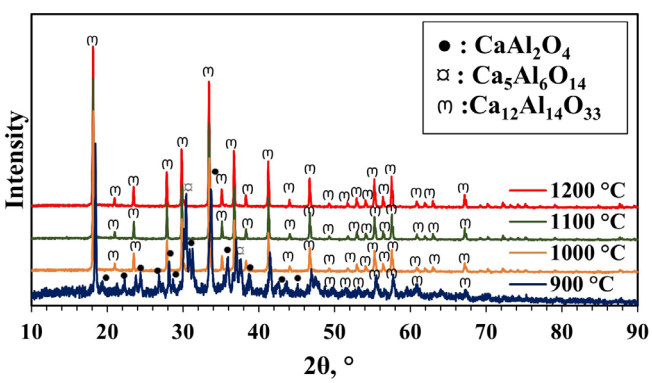

Figure 6. XRD patterns of materials synthesized with pH adjustment and calcined at different temperatures (900–1200 °C) for 4 h (MS:CA 1:2, pH of 1).

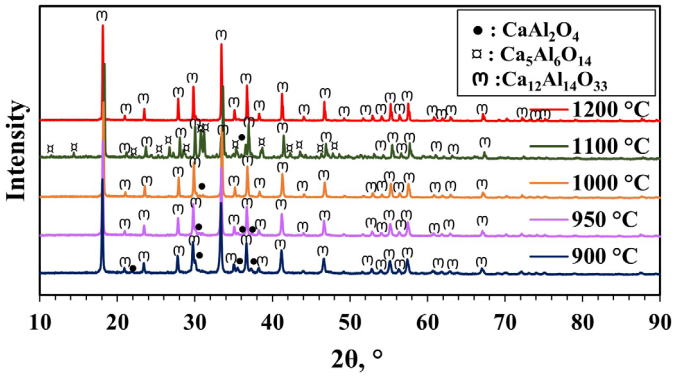

Figure 7. XRD patterns of materials synthesized with pH adjustment and calcined at different temperatures (900–1200 °C) for 4 h (MS:CA 1:2, pH of 2).

At 900 °C, the crystal structure contained much less impurities compared to the materials synthesized with a pH of 0.43 and 1. Unlike other pH levels, the mayenite phase again formed at 1100 °C, but the side phases $Ca_5Al_6O_{14}$ and $CaAl_2O_4$, which are the usual impurities formed during the mayenite synthesis, were also formed. Sanchez et al. [4] also reported the formation of the $Ca_5Al_6O_{14}$ impurity phase in the synthesis of mayenite at a calcination temperature of 1100 °C. When the temperature was increased to 1200 °C, the pure mayenite phase was present without indication of any impurities. Similar to the synthesized materials with other parameters, the crystal size (79.6 nm) of the material was not affected by the change in calcination temperature. Additionally, the crystallinity of the material increased with increasing calcination temperature (except 1100 °C) (Table 1).

TG, N_2 adsorption-desorption, SEM, FTIR, Raman, XPS, pyridine adsorbed DRIFTS, and ICP-OES analyses were carried out with an MS to CA molar ratio of 1:2 and pH 2, where the pure mayenite phase was obtained. The effects of temperature on the structure were investigated by applying the analyses to samples at different calcination temperatures (900–1200 °C). TG analysis of the material with an MS to CA molar ratio of 1:2 and a pH of 2 was carried out at 30–1300 °C with a heating rate of 5 °C/min under dry air flow. Figure 8 displays the findings of the TG analysis investigation of precalcination powder obtained in mayenite synthesis. Weight loss up to 160 °C was caused by water evaporation since organic species are stable below this temperature. Nitrates burn with the remaining simple CA at temperatures between 160 and 275 °C, causing a significant weight loss. Metal citrate complexes break down into metal oxides between 275 and 380 °C, and all organic substances burn through oxidative degradation at temperatures exceeding 380 °C [35]. According to derivative thermogravimetry (DTG), the mass loss that occurs at approximately 373 °C is due to the decomposition of the aluminum nitrate salt into alumina ($2Al(NO_3)_3 \rightarrow Al_2O_3 + NO_2 + O_2$) [2]. At temperatures above 50 °C, CA was used as a chelating agent that reacts with calcium nitrate to form calcium citrate ($3Ca(NO_3)_2.4H_2O + 3C_6H_8O_7 \rightarrow Ca_3(C_6H_5O_7)_2.4H_2O + 3CO_2 + 7H_2O + 6NO_2$). At a temperature of approximately 474 °C, calcium citrate decomposes into calcium carbonate ($Ca_3(C_6H_5O_7)_2 \rightarrow 3CaCO_3 + 5H_2O + 9C$) [45]. Finally, at approximately 919 °C, the calcium carbonate turns into calcium oxide CaO ($CaCO_3 \rightarrow CaO + CO_2$) [2,45]. Salasin et al. [35] achieved a similar TG analysis profile in the synthesis of mayenite using the citrate sol-gel method.

The morphology of the synthesized materials at 900, 1000, 1100, and 1200 °C were investigated by SEM analysis. The images that are shown in Figure 9 display randomly shaped particles in materials synthesized using different calcination temperatures. The increase in calcination temperature makes the structure more homogeneous and regular. Raab et al. [46] obtained a similar structure in the SEM image of synthesized mayenite at 1200 °C.

N_2 adsorption-desorption analysis determined the specific surface area of mayenite materials synthesized at different temperatures. The surface areas of the synthesized materials were less than 1 m^2/g (Table 2). Additionally, there was a decrease in surface area values with increasing temperature. Mironova et al. [47] reported that the specific surface area of the mayenite they synthesized was 0.5 m^2/g.

Raman spectroscopy was used in addition to XRD to verify the phase identity of synthesized mayenite materials. Raman analyses results of the material synthesized with an MS to CA molar ratio of 1:2, a pH of 2, and calcined at 900, 1000, 1100, and 1200 °C are shown in Figure 10. The mayenite material has several modes in the range of 150–1000 cm^{-1} attributed to Al-O framework vibrations. The most dominant mode of mayenite is around 520 cm^{-1}, attributed to the symmetric Al-O-Al vibration of the oxygen bridge between the AlO_4 tetrahedrons. At approximately 311 cm^{-1}, there is an

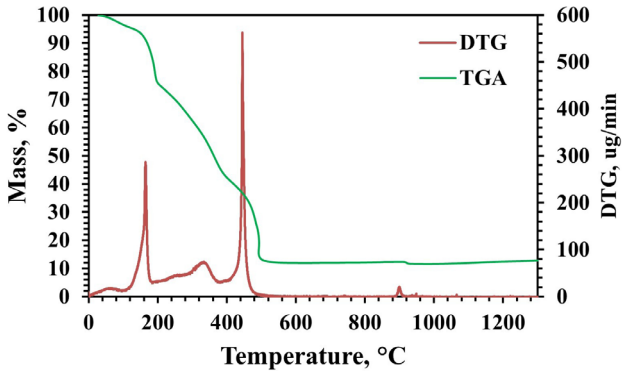

Figure 8. TG analysis results of material synthesized with pH adjustment (MS:CA 1:2, pH of 2). (TGA: thermogravimetric analysis and DTG: derivative thermogravimetry)

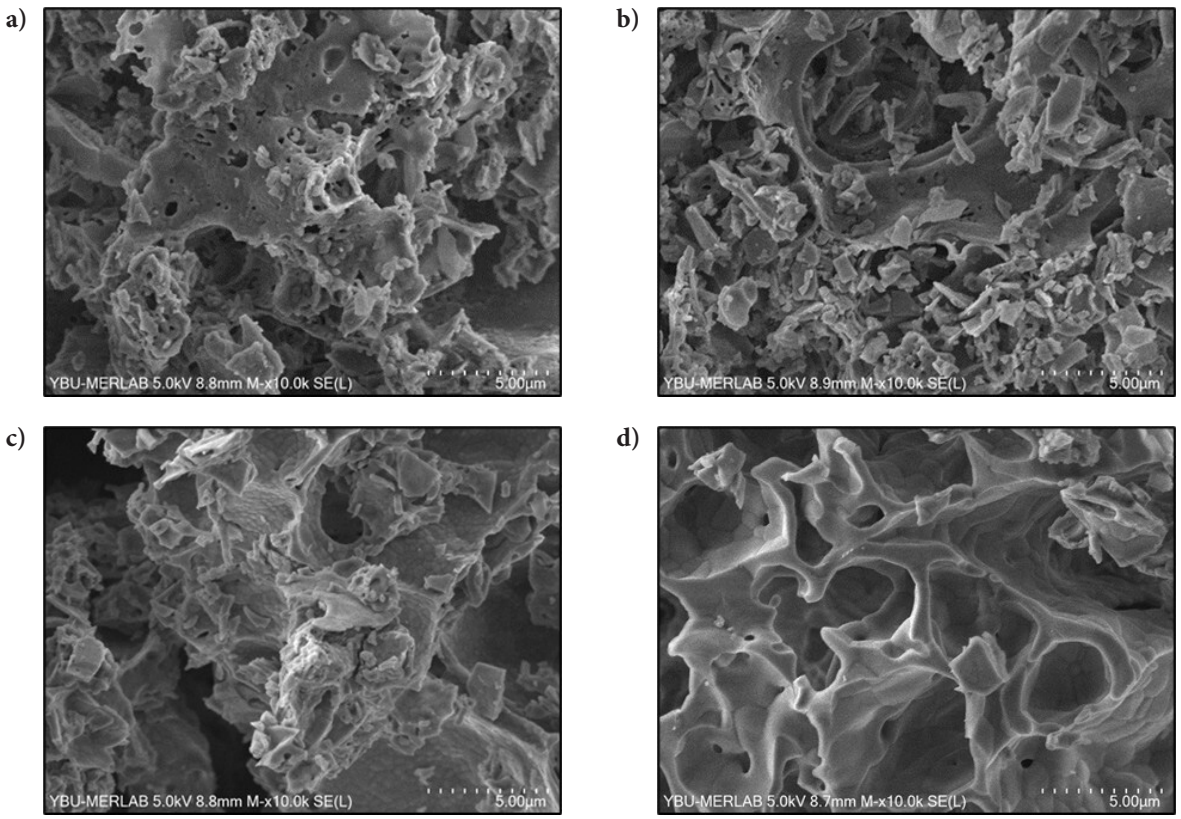

Figure 9. SEM images of materials synthesized with pH adjustment and calcined at different calcination temperatures for 4 h (MS:CA 1:2, pH of 2) (a) 900 °C, (b) 1000 °C, (c) 1100 °C, and (d) 1200 °C.

Table 2. N_2 adsorption-desorption results of materials synthesized with pH adjustment and calcined at different calcination temperatures for 4 h (MS:CA 1:2, pH of 2).

Calcination Temperature, °C	Surface Area, m^2/g
900	0.71
1000	0.52
1100	0.48
1200	0.13

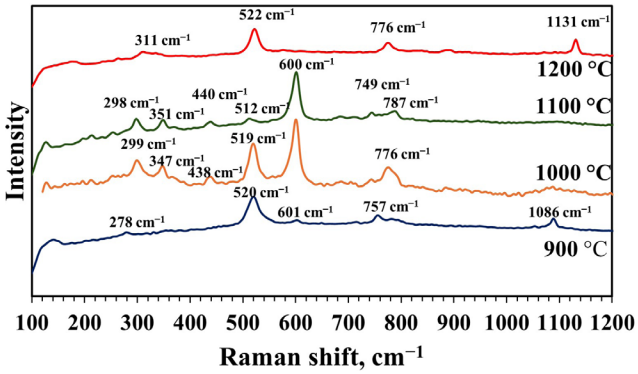

Figure 10. Raman spectra of materials synthesized with pH adjustment and calcined at different calcination temperatures (900–1200 °C) for 4 h (MS:CA 1:2, pH of 2).

additional weaker and broader line that is thought to be caused by framework vibrations. The vibrations seen in the regions around 776 and 1131 cm^{-1} are attributed to the vibrations of the extra framework O_2^- species [14,48–51]. The material synthesized at 900 °C has 2 bands in the Raman spectrum other than the vibrations of pure mayenite material. The high-frequency band at 1086 cm^{-1} can be associated with the O_2^- structure, and the low-frequency band at 278 cm^{-1} is due to a vibrational group in the Ca and O structure. Reports suggest that the band at 1086 cm^{-1} can be attributed to both $CaCO_3$ [50,52] and extra framework oxygen in the structure [53]. XRD results did not indicate $CaCO_3$ in the structure (Figure 7); however, this may have been caused by the crystal size of this phase being too small. The Raman spectra of materials synthesized at 1000 and 1100 °C yielded extra bands around 300, 350, and 440 cm^{-1}. The weak bands at approximately 300 and 350 cm^{-1} may be associated with the Ca-O bond or framework O [51,54]. The weak band at approximately 440 cm^{-1} might originate from the $CaAl_2O_4$ phase in the structure, and this band is related to the AlO_4^{5-} vibration [54]. The sharp band seen at 600 cm^{-1} at both temperatures is the characteristic band of the $Ca_5Al_6O_{14}$ phase [48,51]. In the XRD pattern of the material synthesized at 1100 °C, an excess of $Ca_5Al_6O_{14}$ phase was detected in the structure (Figure 7). This result also supports the XRD analysis result. At 1000 °C, only $CaAl_2O_4$ and $Ca_{12}Al_{14}O_{33}$ phases were detected in the XRD result. The $Ca_5Al_6O_{14}$ phase was not seen in XRD due to the low concentration of the $Ca_5Al_6O_{14}$ phase or small crystal sizes. The Raman spectrum obtained from the calcined material at 1200 °C is in accordance with the pure mayenite spectrum. The XRD pattern of synthesized material at this temperature also shows a pure mayenite phase, which supports the Raman analysis result. The main Raman bands and phase interpretations obtained are given in Table 3.

FTIR spectra were used to evaluate the vibration mode of the atomic bonding of material synthesized with an MS to CA molar ratio of 1:2, a pH of 2, and calcined at 900, 1000, 1100, and 1200 °C (Figure 11). The aluminum coordination number, the coordination group state (isolated or condensed), and the vibrational coupling between adjacent units affect the FTIR spectra of inorganic aluminates. Characteristic IR absorbance frequency ranges are 900–700 cm^{-1} for condensed AlO_4 tetrahedra, 800–650 cm^{-1} for isolated AlO_4 tetrahedra, 680–500 cm^{-1} for condensed AlO_6 octahedra, and 530–400 cm^{-1} for isolated AlO_6 octahedra [55]. The FTIR patterns of calcium aluminate compounds are quite different, but they are characterized by a strong vibration in the region of 900–760 cm^{-1}. This vibration should be associated with AlO_4 tetrahedra or, more specifically, the stretching vibrations of a lattice of interconnected AlO_4 tetrahedra [55]. The peak at 773 cm^{-1} may also be associated with the free oxygen in the framework structure of mayenite. The 572 and 455 cm^{-1} vibrational bands are related to the bonds of Ca, Al, and O atoms (Ca-O-Al stretching) [32]. Some bending motion of the AlO_4 lattice may have contributed to the strong absorption observed in the 400–500 cm^{-1} region.

While similar spectra are obtained at temperatures of 1000 °C and above in the spectra of samples synthesized at different calcination temperatures, band vibrations are weaker or absent at 900 °C. Unlike other temperatures, the vibration observed at 900 °C can be attributed to the Ca-O bond [56]. The conclusion that the vibration seen in the Raman spectrum of 1086 cm^{-1} is caused by $CaCO_3$ can be supported by this result obtained in the FTIR spectrum. Also, in the TG analysis (Figure 8), $CaCO_3$ decomposed into CaO at approximately 919 °C, which may suggest that there is a small amount of $CaCO_3$ left in the structure. As a result, mayenite synthesized at 1000 °C and above has AlO_4-tetrahedral sites, and FTIR spectra show the characteristic peaks for both condensed and isolated AlO_4 tetrahedral peaks.

Pyridine adsorbed DRIFTS analysis was performed to determine the surface acidity of materials synthesized at various calcination temperatures. The vibration bands corresponding to pyridine species were observed in the 1400–1650 cm^{-1}

Table 3. The main Raman bands and their identified phases.

Raman Shift, cm^{-1}	Phase Identity	Assignment	Assignment references
278	$CaCO_3$	Framework Ca	[52]
299, 311	$Ca_{12}Al_{14}O_{33}$	Framework O	[14,51]
347, 351	$Ca_{12}Al_{14}O_{33}$	Framework O	[14,53]
438, 440	$CaAl_2O_4$	Framework Al	[54]
512,519,520,522	$Ca_{12}Al_{14}O_{33}$	Framework O and Al	[14,48–51]
600, 601	$Ca_5Al_6O_{14}$	Framework O and Al	[14,48,51]
749, 757	$Ca_{12}Al_{14}O_{33}$	Framework O, Al	[53]
776, 787	$Ca_{12}Al_{14}O_{33}$	Extra framework O_2^-	[14,48–51]
1086	$Ca_{12}Al_{14}O_{33}$ or $CaCO_3$	Extra framework O_2^- or framework Ca and O	[50,52,53]
1131	$Ca_{12}Al_{14}O_{33}$	Extra framework O_2^-	[14,48–51]

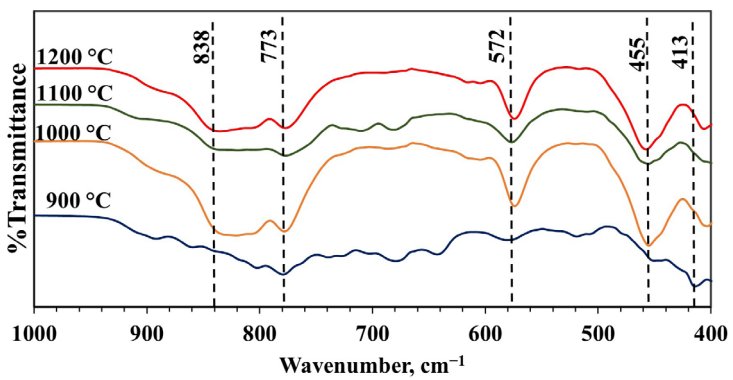

Figure 11. FTIR spectra of materials synthesized with pH adjustment and calcined at different temperatures (900–1200 °C) for 4 h (MS:CA 1:2, pH of 2).

region. Materials did not have peaks in the wave number range of 1400–1650 cm^{-1}, indicating no acidic sites on the synthesized materials (Figure 12).

XPS analysis determined the surface properties of material synthesized with an MS to CA molar ratio of 1:2, pH of 2, and calcined at 1200 °C. XPS spectra were collected for the C 1s, O 1s, Al 2p, and Ca 2p regions of the samples (Figure 13). C 1s peak data were first examined for the configuration and confirmation of XPS spectra. The peak that was positioned after fitting was located at 284.46 eV (Figure 13a) [57]. Deconvolution of the O 1s spectrum shows 2 separate contributions, with peaks located at around 530.5 eV and 531.93 eV, respectively (Figure 13b). The high-energy component at 531.93 eV is attributed to the bridging oxygen (BO) atoms, while the low-energy component at 530.5 eV is assigned to nonbridgeable oxygen (NBO) atoms [58]. The Ca 2p XPS spectra show 2 peaks at around 346.42 eV and 349.86 eV, which are related to Ca $2p_{3/2}$ and Ca $2p_{1/2}$, respectively (Figure 13c). These 2 peaks result from spin-orbit splitting in the Ca 2p XPS spectra. These findings show that Ca and O are linked, creating CaO [58–60]. The Al 2p XPS spectra have peak locations around 73.29 eV, indicating that the valence state of Al (+3) in $Ca_{12}Al_{14}O_{33}$ is the same as that of Al_2O_3 (Figure 13d) [57–60]. It is concluded that the bonds of Ca-O and Al-O exist in the structure of the mayenite synthesized from the resulting XPS spectra.

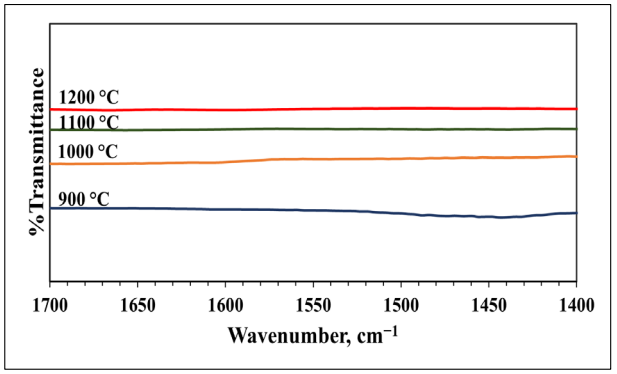

Figure 12. Pyridine adsorbed DRIFTS spectra of materials synthesized with pH adjustment and calcined at different temperatures (900–1200 °C) for 4 h (MS:CA 1:2, pH of 2).

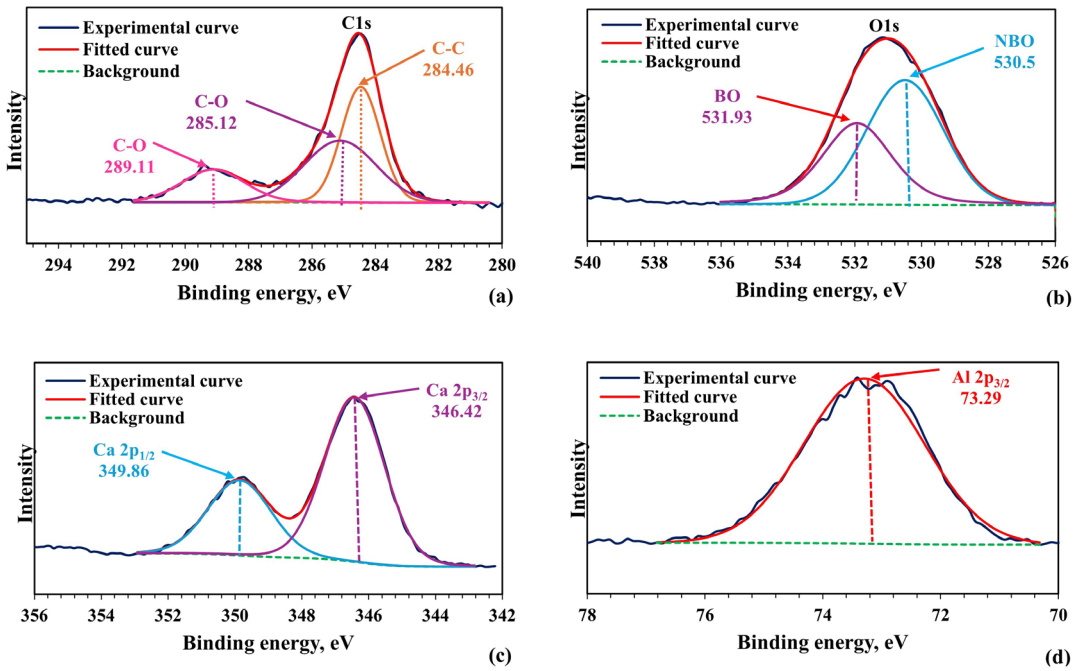

Figure 13. XPS spectra of material synthesized with pH adjustment and calcined at 1200 °C for 4 h (MS:CA 1:2, pH of 2) **(a)** C 1s, **(b)** O 1s, **(c)** Ca 2p and **(d)** Al 2p.

ICP-OES analysis was also conducted to verify the Ca and Al ratios of material synthesized with an MS to CA molar ratio of 1:2, a pH of 2, and calcined at 1200 °C. The ICP-OES analysis shows that the material contained 34 ± 1% Ca and 26 ± 1% Al by weight and was synthesized in the desired ratios.

Abbreviations and their definitions used in this paper are given in Table 4.

4. Conclusions

This study investigated the effects of MS to CA molar ratio, pH, and calcination temperature on the final structure of mayenite synthesized using the citrate sol-gel method. The crystal structure of synthesized materials with different synthesis parameters was investigated using XRD. With the MS to CA ratio of 1, different calcium aluminate phases were formed in materials without pH adjustment; however, mayenite was not formed except at 1000 and 1100 °C. Even at these temperatures, mayenite is not the main phase obtained. When the pH of the solution was adjusted to 2 and the MS to CA ratio is kept at 1, the mayenite phase formed as the dominant phase in the structure at all calcination temperatures. On the

Table 4. List of abbreviations and acronyms used in the article.

Abbreviation	Definition
CA	Citric acid
cm^{-1}	Reciprocal centimeter
DRIFTS	Diffuse reflectance Fourier-transformed infrared spectroscopy
DTG	Derivative thermogravimetry
eV	Electron volt
FTIR	Fourier-transform infrared spectroscopy
ICP-OES	Inductively coupled plasma-optical emission spectrometry
K	Constant in the Scherrer equation
L	Measure of the dimension of the particle in the direction perpendicular to the reflecting plane
MS	Metal salt
nm	Nanometer
SEM	Scanning electron microscopy
TG	Thermogravimetric
XPS	X-ray photoelectron spectroscopy
XRD	X-ray diffraction
β	Full width at half maxima of the strongest peak in the XRD pattern
θ	Angle between the beam and the normal on the reflecting plane
λ	X-ray wavelength

other hand, a significant amount of $Ca_5Al_6O_{14}$, $Ca_3Al_2O_6$, and $CaAl_2O_4$ impurities were also observed in the structure at all temperatures. The crystallinity of the samples increases with increasing calcination temperature, as expected.

This study shows that the MS to CA molar ratio is more important than pH in synthesizing pure mayenite. When the MS to CA ratio was 1:2, mayenite formed as the main phase in the structure at all pH levels and calcination temperatures. With no pH adjustment and the MS to CA ratio of 1:2, there was a $CaAl_2O_4$ impurity phase in the material structure in addition to the mayenite phase at 900 °C. The increase in calcination temperature led to a decrease in this impurity phase and increased crystallinity. With a pH of 1, $Ca_5Al_6O_{14}$ was also observed as an impurity in addition to $CaAl_2O_4$ at 900 °C. By increasing the calcination temperature, the crystallinity in the samples increases and impurities decrease. Above 1000 °C, almost pure mayenite was obtained.

With the MS to CA ratio at 1:2 and a pH of 2, $CaAl_2O_4$ was the only impurity phase at calcination temperatures of 900, 950, and 1000 °C, but it was at a lower level than at a pH of 0.43 and 1. XRD results showed that the sample calcined at 1100 °C had a small amount of $Ca_5Al_6O_{14}$ impurities in its structure besides $CaAl_2O_4$. When the calcination temperature was increased to 1200 °C, no impurities were observed in the structure and pure mayenite was obtained. Crystallinity increased with increasing calcination temperature, reaching a maximum of 87% at 1200 °C. Mayenite crystal sizes was not affected by the synthesis parameters, and it was calculated as 79.6 nm for all samples containing mayenite. The purity of the mayenite structure formed at 1200 °C with a MS to CA ratio of 1:2 and a pH of 2 was confirmed by Raman, FTIR, and XPS analysis in addition to XRD. Moreover, ICP-OES analysis on this sample showed that it contained 34 ± 1% Ca and 26 ± 1% Al by weight, which is compatible with the amounts in mayenite. N_2 adsorption-desorption analysis was also performed on samples synthesized with the MS to CA ratio of 1:2 and pH of 2, showing that the surface area decreased from 0.71 to 0.13 m^2/g as the calcination temperature increased from 900 to 1200 °C, respectively.

In summary, this study establishes the optimal synthesis conditions for mayenite and investigates the impact of various synthesis parameters on its structural properties. The results show that these parameters significantly influence the final crystal structure of mayenite synthesized via the citrate sol-gel method. The most favorable conditions for preparing pure mayenite are an MS to CA molar ratio of 1:2 and calcination temperatures exceeding 1000 °C, with 1200 °C yielding the highest purity. Additionally, pH has less of an effect on the formation of pure mayenite than the MS to CA molar ratio and calcination temperature. The findings of this study offer valuable insights for any research involving mayenite. The synthesis method for pure mayenite presented herein has the potential to significantly improve the performance of various applications, including oxide-conducting electrolytes, fluorescent lamps, moisture sensors, hydrogen-permeable membranes, oxygen pumps, hydrogen storage systems, and catalytic processes.

Acknowledgments
This study was supported by the Scientific and Technological Research Council of Türkiye (TÜBİTAK) TÜBİTAK-BIDEB-2232 Program (118C237), Gazi University Research Fund (FDK-2023-8907), TÜBİTAK 2211 PhD Scholarship Program, and TÜBİTAK 2250 Performance-Based Scholarships Program for PhD. The authors thank the Atılım University Metal Forming Center of Excellence, the Central Laboratory of METU, and the Central Laboratory of AYBU for the characterization results of the synthesized materials.

References

[1] Irvine JTS, West AR. $Ca_{12}Al_{14}O_{33}$ - A possible high-temperature moisture sensor. Journal of Applied Electrochemistry 1989; 19: 410–2. https://doi.org/10.1007/BF01015244

[2] Ude SN, Rawn CJ, Peascoe RA, Kirkham MJ, Jones GL et al. High temperature X-ray studies of mayenite synthesized using the citrate sol-gel method. Ceramics International 2014; 40: 1117–23. https://doi.org/10.1016/j.ceramint.2013.06.112

[3] Khan K, Tareen AK, Aslam M, Thebo KH, Khan U et al. A comprehensive review on synthesis of pristine and doped inorganic room temperature stable mayenite electride, $[Ca_{24}Al_{28}O_{64}]^{4+}(e^-)_4$ and its applications as a catalyst. Progress in Solid State Chemistry 2019; 54: 1–19. https://doi.org/10.1016/j.progsolidstchem.2018.12.001

[4] Lucca Sánchez FA, Lopes de Almeida W, Caldas de Sousa V. An investigation of fuel precursors and calcination temperature to obtain mayenite ($Ca_{12}Al_{14}O_{33}$) powders by solution combustion synthesis. Ceramics International 2023; 49: 15726–33. https://doi.org/10.1016/j.ceramint.2023.01.166

[5] Visbal H, Omura T, Nagashima K, Itoh T, Ohwaki T et al. Exploring the capability of mayenite ($12CaO{\cdot}7Al_2O_3$) as hydrogen storage material. Scientific Reports 2021; 11: 1–11. https://doi.org/10.1038/s41598-021-85540-8

[6] Hu Q, Tan R, Li J, Song W. Highly conductive C12A7:e– electride nanoparticles as an electron donor type promoter to P25 for enhancing photocatalytic hydrogen evolution. Journal of Physics and Chemistry Solids 2021; 149: 109810. https://doi.org/10.1016/j.jpcs.2020.109810

[7] Intiso A, Martinez-Triguero J, Cucciniello R, Proto A, Palomares AE et al. A novel synthetic route to prepare high surface area mayenite catalyst for TCE oxidation. Catalysts 2019; 9: 1–8. https://doi.org/10.3390/catal9010027

[8] Li C, Hirabayashi D, Suzuki K. Synthesis of higher surface area mayenite by hydrothermal method. Materials Research Bulletin 2011; 46: 1307–10. https://doi.org/10.1016/j.materresbull.2011.03.023

[9] Berent K, Komarek S, Lach R, Pyda W. The effect of calcination temperature on the structure and performance of nanocrystalline mayenite powders. Materials 2019; 12. https://doi.org/10.3390/ma12213476

[10] Boysen H, Kaiser-bischoff I, Lerch M, Berendts S, Hoelzel M. Disorder and diffusion in mayenite. Acta Physica Polonica A 2010; 117: 38–41. https://doi.org/10.12693/APhysPolA.117.38

[11] Boysen H, Lerch M, Berendts S, Börger A, Trots DM et al. Structures and properties of variously doped Mayenite investigated by neutron and synchrotron powder diffraction. Zeitschrift fur Kristallographie 2009; 30: 323–8. https://doi.org/10.1524/9783486992588-051

[12] Khan K, Tareen AK, Aslam M, Khan SA, Khan Q et al. Fe-doped mayenite electride composite with 2D reduced Graphene Oxide : As a non-platinum based, highly durable electrocatalyst for Oxygen Reduction Reaction. Scientific Reports 2019; 9: 1–11. https://doi.org/10.1038/s41598-019-55207-6

[13] Lacerda M, Irvine JTS, Glasser FP, West AR. High oxide ion conductivity in $Ca_{12}Al_{14}O_{33}$. Nature 1988; 332: 525–6. https://doi.org/10.1038/332525a0

[14] Eufinger JP, Schmidt A, Lerch M, Janek J. Novel anion conductors - Conductivity, thermodynamic stability and hydration of anion-substituted mayenite-type cage compounds C12A7:X (X = O, OH, Cl, F, CN, S, N). Physical Chemistry Chemical Physics 2015; 17: 6844–57. https://doi.org/10.1039/c4cp05442c

[15] Lee DK, Kogel L, Ebbinghaus SG, Valov I, Wiemhoefer HD et al. Defect chemistry of the cage compound, $Ca_{12}Al_{14}O_{33-\delta}$ - Understanding the route from a solid electrolyte to a semiconductor and electride. Physical Chemistry Chemical Physics 2009; 11: 3105–14. https://doi.org/10.1039/b818474g

[16] Hayashi K, Hirano M, Hosono H. Thermodynamics and kinetics of hydroxide ion formation in $12CaO{\cdot}7Al_2O_3$. Journal of Physical Chemistry B 2005; 109: 11900–6. https://doi.org/10.1021/jp050807j

[17] Jiang D, Zhao Z, Mu S, Qian H, Tong J. Facile and massive aluminothermic synthesis of mayenite electrides from cost-effective oxide and metal precursors. Inorganic Chemistry 2019; 58: 960–7. https://doi.org/10.1021/acs.inorgchem.8b03116

[18] Li F, Zhang X, Liu H. Insights into the direct formation of $[Ca_{24}Al_{28}O_{64}]^{4+}(4e-)$ and its electrical characterization. Journal of the American Ceramic Society 2020; 103: 35–42. https://doi.org/10.1111/jace.16769

[19] Schmidt A, Boysen H, Senyshyn A, Lerch M. New findings on N-mayenite and a new kind of anion substituted mayenite: $Ca_{12}Al_{14}O_{32}(NO_2)_2$. Zeitschrift Fur Kristallographie 2014; 229: 427–34. https://doi.org/10.1515/zkri-2013-1720

[20] Yang S, Kondo JN, Hayashi K, Hirano M, Domen K et al. Formation and desorption of oxygen species in nanoporous crystal $12CaO{\cdot}7Al_2O_3$. Chemistry of Materials 2004; 16: 104–10. https://doi.org/10.1021/cm034755r

[21] Huang F, Li J, Wang L, Dong T, Tu J et al. Features and mechanism of H^- anion emission from $12CaO{\cdot}7Al_2O_3$ surface. Journal of Physical Chemistry B 2005; 109: 12032–7. https://doi.org/10.1021/jp050006g

[22] Ozawa K, Sakamoto N, Wakiya N, Suzuki H. Fabrication of $12CaO{\cdot}7Al_2O_3$ powders with high specific surface area by sol – gel and ball-milling method. Journal of the Ceramic Society of Japan 2011; 119: 460-463. https://doi.org/10.2109/jcersj2.119.460

[23] Asiltürk M, Sayilkan F, Içduygu G, Sayilkan H. The synthesis and applications of Cr-doped GLYMO and GLYMO/DAMO surface coating systems for absorbing UV-light by sol-gel process. Turkish Journal of Chemistry 2005; 29: 83–93

[24] Sayilkan F, Sayilkan H, Erdemoğlu S, Şener Ş, Akarsu M. New adsorbents from $Ti(OPrn)_4$ by the sol-gel process: Synthesis, characterization and application for removing some heavy metal ions from aqueous solution. Turkish Journal of Chemistry 2004; 28: 27–38

[25] Hamdi D, Mansouri L, Srivastava V, Sillanpaa M, Bousselmi L. Cerium and europium doped TiO_2 thin films deposited by a sol-gel dip-coating process: characterization and photocatalytic activity toward dye degradation. Turkish Journal of Chemistry 2022; 46: 415–33. https://doi.org/10.55730/1300-0527.3317

[26] Parashar M, Shukla VK, Singh R. Metal oxides nanoparticles via sol–gel method: a review on synthesis, characterization and applications. Journal of Materials Science: Materials in Electronics 2020; 31: 3729–49. https://doi.org/10.1007/s10854-020-02994-8

[27] Ahmadi H, Khalaj G, Najafi A, Abbasi SM, Safari M. Metakaolin-red mud / carbon nanotubes geopolymer nanocomposite : mechanical properties and structural studies. Materials Research Express 2022; 9: 025011. https://doi.org/10.1088/2053-1591/ac54d6

[28] Mahmoudi Z, Mesgari Abbasi S, Soleymani F, Khalaj G, Najafi A. Development of sol-gel synthesis and characterization of meso porous SiO_2 nanopowder for improvement of nanomullite/SiC ceramic filter. Ceramics International 2024; 51: 4918–28. https://doi.org/10.1016/j.ceramint.2024.11.464

[29] Morshed M, Najafi A, Khalaj G. Exploring the impact of pH and temperature on TiC nanopowders syntesized via sol-gel and subsequent crystallization by carbothermal reduction method. Physica Scripta 2024; 99: 035966. https://doi.org/10.1088/1402-4896/ad2acc

[30] Fu X, Niu Z, Peng C, Han H, Sun W et al. Quantitative synergistic adsorption affinity of Ca(II) and sodium oleate to predict the surface reactivity of hematite and quartz. Separation and Purification Technology 2025; 360: 131196. https://doi.org/10.1016/j.seppur.2024.131196

[31] Drabczyk A, Kudłacik-Kramarczyk S, Korniejenko K, Figiela B, Furtos G. Review of geopolymer nanocomposites: Novel materials for sustainable development. Materials 2023; 16: 3478. https://doi.org/10.3390/ma16093478

[32] Sriwong C, Phrompet C, Tuichai W, Karaphun A, Kurosaki K et al. Synthesis, microstructure, multifunctional properties of mayenite $Ca_{12}Al_{14}O_{33}$ (C12A7) cement and graphene oxide (GO) composites. Scientific Reports 2020; 10: 1–19. https://doi.org/10.1038/s41598-020-68073-4

[33] Danks AE, Hall SR, Schnepp Z. The evolution of "sol-gel" chemistry as a technique for materials synthesis. Materials Horizons 2016; 3: 91–112. https://doi.org/10.1039/c5mh00260e

[34] Suhasinee Behera P, Bhattacharyya S, Sarkar R. Effect of citrate to nitrate ratio on the sol-gel synthesis of nanosized α-Al_2O_3 powder. Ceramics International 2017; 43: 15221–6. https://doi.org/10.1016/j.ceramint.2017.08.057

[35] Salasin JR, Schwerzler SEA, Koehler MR, Keffer DJ, Rawn CJ. The effect of process parameters on the amorphous citrate sol-gel synthesis of Cu-doped $Ca_{12}Al_{14}O_{33}$. Materialia 2018; 4: 466–77. https://doi.org/10.1016/j.mtla.2018.11.003

[36] Imanasa F, Yang Y, Panias D, Kolbeinsen L, Safarian J. Leaching characteristics and mechanism of the synthetic calcium-aluminate slags for alumina recovery. Hydrometallurgy 2019; 185: 273–90. https://doi.org/10.1016/j.hydromet.2019.03.006

[37] Eryildirim B, Arbag H, Oktar N, Dogu G. Comparison of microwave and conventionally heated reactor performances in catalytic dehydrogenation of ethane. International Journal of Hydrogen Energy 2021; 46: 5296–310. https://doi.org/10.1016/j.ijhydene.2020.11.067

[38] Ilyina EV, Bedilo AF, Cherepanova SV, Gerus YY, Shuvarakova EI et al. Aerogel synthesis of calcium aluminates with varied stoichiometry. Journal of Sol-Gel Science and Technology 2022; 104: 259–66. https://doi.org/10.1007/s10971-022-05933-7

[39] Steele FA, Davey WP. The crystal structure of tricalcium aluminate. The Journal of the Association Chemical Society 1864; 84: 730–1. https://doi.org/10.1021/ja01383a001

[40] Hörkner W, Müller-Buschbaum H. Zur kristallstruktur von $CaAl_2O_4$. Journal of Inorganic and Nuclear Chemistry 1976; 38: 983–4. https://doi.org/10.1016/0022-1902(76)80011-5 (in German)

[41] Cucciniello R, Intiso A, Castiglione S, Genga A, Proto A et al. Total oxidation of trichloroethylene over mayenite ($Ca_{12}Al_{14}O_{33}$) catalyst. Applied Catalysis B : Environmental 2017; 204: 167–72. https://doi.org/10.1016/j.apcatb.2016.11.035

[42] Boysen H, Lerch M, Stys A, Senyshyn A. Structure and oxygen mobility in mayenite ($Ca_{12}Al_{14}O_{33}$): A high-temperature neutron powder diffraction study. Acta Crystallographica Section B: Structural Science, Crystal Engineering and Materials 2007; 63: 675–82. https://doi.org/10.1107/S0108768107030005

[43] Vincent MG, Jeffery JW. The crystal structure of pentacalcium trialuminate, $5CaO.3AI_2O_3$. Acta Crystallographica Section B: Structural Science, Crystal Engineering and Materials 1978; B34: 1422–1428. https://doi.org/10.1107/S0567740878005828

[44] Intiso A, Martinez-Triguero J, Cucciniello R, Rossi F, Palomares AE. Influence of the synthesis method on the catalytic activity of mayenite for the oxidation of gas-phase trichloroethylene. Scientific Reports 2019; 9: 1–9. https://doi.org/10.1038/s41598-018-36708-2

[45] Mansour SAA. Thermal decomposition of calcium citrate tetrahydrate. Thermochimica Acta 1994; 233: 243–56. https://doi.org/10.1016/0040-6031(94)85118-2

[46] Raab B, Poellmann H. Heat flow calorimetry and SEM investigations to characterize the hydration at different temperatures of different $12CaO{\cdot}Al_2O_3$ (C12A7) samples synthesized by solid state reaction, polymer precursor process and glycine nitrate process. Thermochimica Acta 2011; 513: 106–11. https://doi.org/10.1016/j.tca.2010.11.019

[47] Mironova EY, Ermilova MM, Orekhova NV, Tolkacheva AS, Shkerin SN et al. Transformations of ethanol on catalysts based on nanoporous calcium aluminate–mayenite ($Ca_{12}Al_{14}O_{33}$) and mayenite doped by copper. Nanotechnologies in Russia 2017; 12: 597–604. https://doi.org/10.1134/S1995078017060064

[48] Spadoni A, Sau S, Corsaro N, Lanchi M, Tizzoni AC et al. Thermochemical heat storage through CaO-Mayenite/$CaCO_3$ system: Thermal performances comparison for two synthesis methods. Journal of Energy Storage 2023; 72: 108386. https://doi.org/10.1016/j.est.2023.108386

[49] Maurelli S, Ruszak M, Witkowski S, Pietrzyk P, Chiesa M et al. Spectroscopic CW-EPR and HYSCORE investigations of $Cu2^+$ and O^{2-} species in copper doped nanoporous calcium aluminate ($12CaO{\cdot}7Al_2O_3$). Physical Chemistry Chemical Physics 2010; 12: 10933–41. https://doi.org/10.1039/c0cp00084a

[50] Shuvarakova EI, Ilyina EV, Stoyanovskii VO, Veselov GB, Bedilo AF et al. Exploration of optical, redox, and catalytic properties of vanadia-mayenite nanocomposites. Journal of Composites Science 2022; 6: 308. https://doi.org/10.3390/jcs6100308

[51] Ruszak M, Witkowski S, Pietrzyk P, Kotarba A, Sojka Z. The role of intermediate calcium aluminate phases in solid state synthesis of mayenite ($Ca_{12}Al_{14}O_{33}$). Functional Materials Letters 2011; 4: 183–6. https://doi.org/10.1142/S1793604711001907

[52] Schmida T, Dariz P. Shedding light onto the spectra of lime: Raman and luminescence bands of CaO, $Ca(OH)_2$ and $CaCO_3$. Journal of Raman Spectroscopy 2014; 46: 141–6. https://doi.org/10.1002/jrs.4622

[53] Veiga FCT, González RF, Egea JJ, da Silva Cava S, de Sousa VC. Mixed electrical conduction of calcium aluminates synthesized by polymeric precursors. Materials Research 2020; 22: 1–12. https://doi.org/10.1590/1980-5373-MR-2018-0271

[54] Torréns-Martín D, Fernández-Carrasco L, Martínez-Ramírez S. Hydration of calcium aluminates and calcium sulfoaluminate studied by Raman spectroscopy. Cement and Concrete Research 2013; 47: 43–50. https://doi.org/10.1016/j.cemconres.2013.01.015

[55] Tarte P. Infra-red spectra of inorganic aluminates and characteristic vibrational frequencies of AlO_4 tetrahedra and AlO_6 octahedra. Spectrochimica Acta Part A: Molecular Spectroscopy 1967; 23: 2127–43. https://doi.org/10.1016/0584-8539(67)80100-4

[56] Jia Y, Wang Y, Jiang C, Wang X, Hu Z et al. Simultaneous enhancement of the H_2 yield and HCl removal efficiency from pyrolysis of infusion tube under novel mayenite-based mesoporous catalytic sorbents. Energy 2022; 244: 123067. https://doi.org/10.1016/j.energy.2021.123067

[57] Khan K, Khan Tareen A, Li J, Khan U, Nairan A et al. Facile synthesis of tin-doped mayenite electride composite as a non-noble metal durable electrocatalyst for oxygen reduction reaction (ORR). Dalton Transactions 2018; 47: 13498–506. https://doi.org/10.1039/c8dt02548g

[58] Pan RK, Feng S, Tao HZ. XPS and NMR analysis on 12CaO•7Al2O3. IOP Conference Series: Materials Science and Enginerring 2017; 167: 012017. https://doi.org/10.1088/1757-899X/167/1/012017

[59] Ruttanapun C, Srepusharawoot P, Maensiri S. Effect of Fe^{3+}-doped $Ca_{12}Al_{14}O_{33}$ cement on optical and thermal properties. Chinese Journal of Physics 2018; 56: 252–60. https://doi.org/10.1016/j.cjph.2017.12.022

[60] Khan K, Tareen AK, Elshahat S, Muhammad N, Li J et al. Facile metal-free reduction-based synthesis of pristine and cation-doped conductive mayenite. RSC Advances 2018; 8: 24276–85. https://doi.org/10.1039/c8ra02790k